

Synthesis of hollow mesoporous silica nanoparticles with tunable shell thickness and pore size using amphiphilic block copolymers as core templates

Cite this: *Dalton Trans.*, 2014, **43**, 11834

Xiaojun Zhou,^{a,b} Xiao Cheng,^a Wei Feng,^a Kexin Qiu,^{a,b} Liang Chen,^a Wei Nie,^a Zhiqi Yin,^a Xiumei Mo,^{a,b} Hongsheng Wang^a and Chuanglong He^{*a}

This paper presents a facile method for the fabrication of uniform hollow mesoporous silica nanoparticles (HMSNs) with tunable shell thickness and pore size. In this method, a series of amphiphilic block copolymers of polystyrene-*b*-poly (acrylic acid) (PS-*b*-PAA) with different hydrophobic block (PS) lengths were first synthesized *via* atom transfer radical polymerization (ATRP). The as-synthesized PS-*b*-PAA and cetyltrimethylammonium bromide (CTAB) were subsequently used as co-templates to fabricate HMSNs. This approach allows the control of shell thickness and pore size distribution of the synthesized HMSNs simply by changing the amounts of PS-*b*-PAA and CTAB, respectively. *In vitro* cytotoxicity and hemolysis assays demonstrated that the synthesized HMSNs had a low and shell thickness-dependent cytotoxicity and hemolytic activity. Therefore, these HMSNs have great potential for biomedical applications due to their good biocompatibility and ease of synthesis.

Received 17th April 2014,
Accepted 11th June 2014

DOI: 10.1039/c4dt01138d

www.rsc.org/dalton

Introduction

Mesoporous silica nanoparticles (MSNs) have attracted a tremendous amount of attention in recent years, due to their unique properties of large specific surface area and pore volume, adjustable pore diameter, facile surface functionalization and excellent biocompatibility.^{1–3} All of these intrinsic properties make MSNs ideal candidates for many potential applications such as catalysis,⁴ separation,^{5,6} drug delivery^{2,7,8} and so on. Particularly, hollow mesoporous silica nanoparticles (HMSNs) that combine a special structure with a hollow core and mesoporous shell have recently emerged as excellent carriers for various bioactive molecules and therapeutic drugs. HMSNs tend to have much higher guest-loading capacity than the solid MSNs owing to their large void core. In addition, they also possess low density, narrow pore size distribution and more advantages in mass diffusion and transportation than conventional solid MSNs.^{9,10} Considerable recent efforts have been devoted to the synthesis of HMSNs with controlled structures and high loading capacity.^{11–14}

The general approach to generate the hollow cavity in MSNs involves a template-driven synthesis process,^{12,15–18} where various hard templates^{18–20} (polymer, carbon and silica particles) and soft templates^{13,21,22} (emulsions, vesicles and micelles) are usually employed. In the case of the hard template method, although hollow silica particles with a well-defined sphere and smooth surface are easily obtained, a rather complex and time-consuming template removal procedure is required.¹⁵ The major limitation of the soft template method is that it is difficult to control the aggregate morphology of soft templates such as vesicles and micelles, which typically result in the irregular and aggregation of the resulting HMSNs.¹⁴ It still remains a challenge to establish a simple and efficient method to synthesize HMSNs.

Since 1992,²³ the amphiphilic block copolymer, polystyrene-*b*-poly (acrylic acid) (PS-*b*-PAA), has been widely investigated for various applications. For example, PS-*b*-PAA was used to immobilize enzymes due to the existence of carboxyl groups.²⁴ It can also self-assemble to form highly ordered microporous thin films and different micellar structures in the selective solvents.^{25–27} Previous studies have demonstrated that PS-*b*-PAA could form micelles with various morphologies in appropriate solvents, including spheres, rods, lamellae and vesicles.^{27,28} However, these morphologies can be affected by various factors, such as the composition of the block copolymers, copolymer concentration, and temperature.²⁹ Niu *et al.* reported the fabrication of core-shell structured dual-meso-

^aCollege of Chemistry, Chemical Engineering and Biotechnology, State Key Laboratory for Modification of Chemical Fibers and Polymer Materials, Donghua University, Shanghai 201620, People's Republic of China. E-mail: hcl@dhu.edu.cn

^bCollege of Materials Science and Engineering, Donghua University, Shanghai 201620, People's Republic of China

porous silica spheres using different PS block lengths of PS-*b*-PAA with rods.³⁰ However, very few studies have been reported so far using PS-*b*-PAA self-assembled micelles as templates to synthesize HMSNs.^{14,30} In this context, it is attractive to fabricate HMSNs using the spherical structure of PS-*b*-PAA micelles.

Herein, we report a facile route to synthesize uniform and monodispersed HMSNs using PS-*b*-PAA and cetyltrimethylammonium bromide (CTAB) as the co-templates. In this method, the shell thickness and pore size of HMSNs could be easily controlled by changing the amounts of PS-*b*-PAA and the surfactant CTAB, respectively. The physical properties of the synthesized HMSNs were characterized with various methods. We also investigated the effects of the shell thickness and pore size of HMSNs on the cytotoxicity of human cervical cancer cells (HeLa cells) and the hemolytic activity of human red blood cells (RBCs).

Experimental

Materials

Styrene (99%), *t*-butyl acrylate (98%), *N,N,N',N''*-penta-methyldiethylenetriamine methyl (PMDETA; 99%), methyl-2-bromopropionate (98%), cetyltrimethylammonium bromide (99%), tetraethyl orthosilicate (TEOS; 99%), *p*-aminobenzene sulfonic acid (99%), and Cu(I)Br (99.999%) were all purchased from Sigma-Aldrich (Shanghai) Trading Co., Ltd (Shanghai, China). Tetrahydrofuran (THF) and aqueous ammonia solution (25 wt%) were purchased from Sinopharm Chemical Reagent Co. Ltd (Shanghai, China). Styrene and *t*-butyl acrylate were dried over CaH₂ and then distilled under reduced pressure at 60 °C and 55 °C, respectively. The distilled monomers were then stored at 4 °C. All other chemicals were used without further purification.

Synthesis of PS-*b*-PAA

The amphiphilic block copolymer PS-*b*-PAA was synthesized *via* sequential atomic transfer radical polymerization (ATRP) as previously reported.³¹

Synthesis of poly(*t*-butyl acrylate) (PtBA)

264 mg of Cu(I)Br, 12 ml of *t*-butyl acrylate, 2.05 ml of methyl-2-bromopropionate and 0.383 ml of PMDETA were transferred into a three-neck round-bottom flask. Then the flask was immersed in a liquid nitrogen bath, and the mixture was exposed to three cycles of freeze-pump-thaw with nitrogen flow to remove the dissolved gas. The mixture was allowed to stir at room temperature until the mixture became homogeneous. The flask was immersed in a 60 °C oil bath and allowed to polymerize with stirring under nitrogen flow. After 6 h, the flask was immersed in liquid nitrogen to quench the polymerization, and 50 ml of acetone was added to dissolve the product. The blue solution was passed through a column of neutral alumina three times to yield a colorless solution. Subsequently, evaporation of the solvent under vacuum was

conducted to yield viscous polymer oil. Finally, after drying under vacuum for 2 days, the polymer PtBA₄ ($\bar{M}_n = 510$, $\bar{M}_w/\bar{M}_n = 1.22$) was synthesized.

Synthesis of PtBA-*b*-PS

129 mg of Cu(I)Br, 1.5 g of PtBA, 15 ml of styrene and 189.9 μl of PMDETA were added into a three-neck round-bottom flask, which was then degassed *via* three cycles of freeze-pump-thaw. The mixture was allowed to stir for 3.5 h at 95 °C under nitrogen flow. Then the flask was immersed in liquid nitrogen to quench the polymerization, and 50 ml of acetone was added to dissolve the product. The blue solution was passed through a column of neutral alumina three times to obtain a transparent solution. The white polymer was then isolated by adding methanol to precipitate and collected by centrifugation (8000 r min⁻¹, 20 min). The final white polymer was dried under vacuum for 2 days. Thus, the PtBA₄-*b*-PS₅₈ ($\bar{M}_n = 6590$, $\bar{M}_w/\bar{M}_n = 1.13$) was synthesized. The molar ratio between Cu(I)Br, PtBA, styrene and PMDETA was changed to 10 : 33.3 : 911.1 : 100 and 10 : 16.7 : 911.1 : 10 respectively, and then PtBA₄-*b*-PS₃₅ ($\bar{M}_n = 4200$, $\bar{M}_w/\bar{M}_n = 1.28$) and PtBA₄-*b*-PS₁₁₃ ($\bar{M}_n = 12\,300$, $\bar{M}_w/\bar{M}_n = 1.20$) were obtained.

Hydrolysis of PtBA-*b*-PS to PS-*b*-PAA

4 g of PtBA-*b*-PS and 0.1 g of *p*-aminobenzene sulfonic acid were dissolved in 100 ml of toluene. Then the mixture was refluxed for 24 h at 110 °C. Finally, the white polymer was isolated by twice of methanol-precipitation and collected by centrifugation (8000 r min⁻¹, 20 min). The obtained product was dried under vacuum over 2 days. Thus, the PS₃₅-*b*-PAA₄, PS₅₈-*b*-PAA₄ and PS₁₁₃-*b*-PAA₄ were respectively synthesized.

Synthesis of HMSNs

For the synthesis of HMSNs, a typical "sol-gel" method was used with PS-*b*-PAA and CTAB as the co-templates, and TEOS as the silica resource. 200 mg of CTAB was dissolved in 80 ml of deionized water, and then 3 ml of aqueous ammonia solution (25 wt%) was added to the solution. After that, 100 mg of PS-*b*-PAA dissolved in 16 ml of THF was added dropwise to the mixture solution. After stirring for 10 min, 140 ml of ethanol was added and allowed to stir for 10 min. Then, 20 ml of ethanol solution containing 0.605 ml of TEOS was added dropwise and the resulting mixture was stirred at room temperature for 24 h. The products were collected by centrifugation (8000 r min⁻¹, 10 min), dried in air, and calcined at 550 °C for 6 h to remove the templates. The same procedures were used to prepare the other HMSNs with different shell thicknesses and pore sizes, and the amount of reactants is shown in Table 1.

Characterization

The as-synthesized nanoparticles were visualized using a JEM-2100F (Jeol Ltd, Japan) transmission electron microscope (TEM) and a Hitachi S-4800 (Hitachi Ltd, Japan) scanning electron microscope (SEM). Gel permeation chromatography/light scattering (GPC/LS) on polymers was performed on a BI-MwA system (Brookhaven, USA). Fourier transform infrared (FT-IR)

Table 1 Synthesis of HMSN samples with different shell thicknesses and pore sizes

Samples	Core template PS _x - <i>b</i> -PAA ₄	Core template amount (mg)	CTAB amount (mg)	TEOS amount (ml)
HMSN-PS ₃₅	X = PS ₃₅	100	200	0.605
HMSN-PS ₅₈	X = PS ₅₈	100	200	0.605
HMSN-PS ₁₁₃	X = PS ₁₁₃	100	200	0.605
HMSN-PS ₃₅ -a	X = PS ₃₅	80	200	0.605
HMSN-PS ₃₅ -b	X = PS ₃₅	75	200	0.605
HMSN-PS ₃₅ -c	X = PS ₃₅	70	200	0.605
HMSN-PS ₅₈ -a	X = PS ₅₈	100	160	0.605
HMSN-PS ₅₈ -b	X = PS ₅₈	100	180	0.605
HMSN-PS ₅₈ -c	X = PS ₅₈	100	200	0.605
HMSN-PS ₅₈ -d	X = PS ₅₈	100	240	0.605

spectra were recorded on a Nicolet 6700 (Thermo, USA). Small-angle X-ray diffraction (XRD) patterns were obtained using a D/MAX-2550PC (Rigaku Inc., Japan) diffractometer with the Cu K α radiation at 45 kV and 40 mA. Surface properties were determined by nitrogen adsorption-desorption measurements with a V-Sorb 2800P (Micromeritics, USA) surface area and pore size analyzer. Pore size distribution and specific surface areas were measured by the Barrett-Joyner-Halenda (BJH) and Brunauer-Emmett-Teller (BET) methods, respectively. The size distribution of the nanoparticles was measured by dynamic light scattering (DLS) using a BI-200SM multi-angle dynamic/static laser scattering instrument (Brookhaven, USA). The hemolytic activity was determined using a UV-vis spectrophotometer (JASCO V-530).

In vitro cytotoxicity assays

The cytotoxicity of HMSNs in various concentrations was investigated using Cell Counting Kit-8 (CCK-8) assays. Briefly, HeLa cells were seeded in 96-well plates with 100 μ l of medium at a density of 1×10^4 cells per well, and cultured in 5% CO₂ at 37 °C for 24 h. The cells were washed with PBS, and various concentrations of HMSNs (1, 10, 25, 50, 100, 200, 400 and 800 μ g ml⁻¹) suspended in culture medium were separately introduced into the cells. After incubation for 24 h, 10 μ l of CCK-8 solution was added, and the cells were incubated for another 2 h at 37 °C. The absorbance was measured at 450 nm with a plate reader (Multiskan MK3, Thermo). A culture medium without nanoparticles was used as the blank control.

The cytotoxicity was expressed as the percentage of the cell viability as compared with the blank control.

Hemolysis assays

Fresh human blood stabilized with heparin was kindly supplied by the Shanghai First People's Hospital (Shanghai, China). The plasma was removed from blood by centrifugation at 3000 r min⁻¹ for 10 min, and the RBCs were washed three times with PBS solution. Then the RBCs were diluted with PBS solution up to a concentration of 10% (w/v). 0.3 ml of diluted RBCs was incubated with 1.2 ml of different HMSN concentrations (25, 50, 100, 200, 400 and 800 μ g ml⁻¹). Distilled water and PBS were served as positive and negative controls, respectively. After incubation at 37 °C for 3 h, the samples were centrifuged (3000 r min⁻¹, 10 min). Then, the supernatant was collected and the absorbance values were measured using a UV-vis spectrophotometer at 541 nm. The percent hemolysis of RBCs in each sample was calculated by the following formula: hemolysis % = [(sample absorbance - negative control) / (positive control - negative control)] \times 100%, and the average value was obtained from five parallel samples.

Statistical analysis

In all the experiments, at least three samples were performed, and the values were expressed as the mean \pm standard deviation (S.D). The statistical analysis was carried out using the one-way analysis of variance (one-way ANOVA). The criteria for statistical significance were * P < 0.05 and ** P < 0.01.

Results and discussion

Preparation and characterization of PS-*b*-PAA and HMSNs

PS-*b*-PAA was synthesized *via* ATRP, and the lengths of the component blocks were determined by GPC. Prior to synthesis of HMSNs, the aggregate morphologies of PS-*b*-PAA samples were characterized by SEM and DLS. Fig. 1 presents the SEM images of PS-*b*-PAA, which is prepared by dissolving copolymers in a selective solvent mixture of THF and water. The aggregate morphologies of the three block copolymers show well-defined spherical micelles with smooth surface. When the hydrophilic PAA block length was 4, while the hydrophobic PS block length in PS-*b*-PAA increased from 35 to 113, the dia-

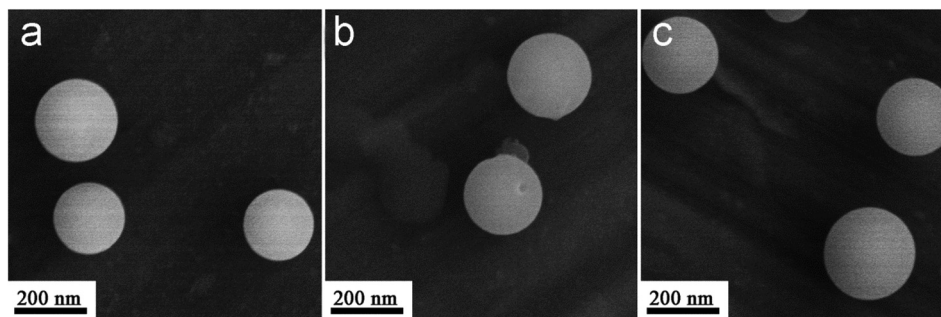


Fig. 1 SEM images of block copolymers PS-*b*-PAA: (a) PS₃₅-*b*-PAA₄, (b) PS₅₈-*b*-PAA₄ and (c) PS₁₁₃-*b*-PAA₄.

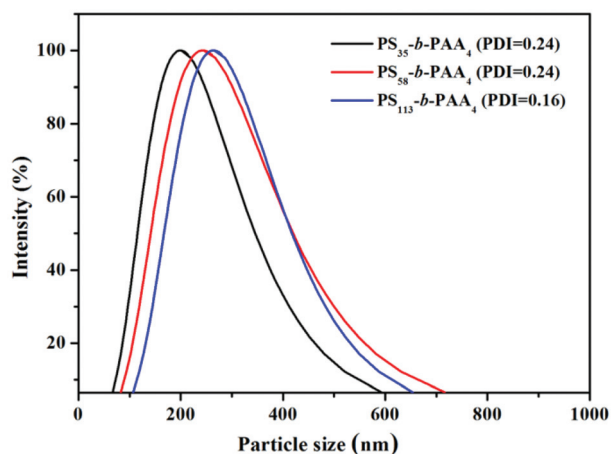


Fig. 2 Size distribution curves of PS₃₅-*b*-PAA₄, PS₅₈-*b*-PAA₄ and PS₁₁₃-*b*-PAA₄.

meter of the spherical micelles was increased from 199.4 to 264.1 nm (Fig. 2). It is known that amphiphilic diblock copolymers can self-assemble to form aggregates with varied morphologies in selective solvents,^{27,28} and the micellization and morphologies of amphiphilic block copolymers are easily affected by various factors.³² In the present study, spherical micelles of PS-*b*-PAA with different PS block lengths were obtained, and the morphology is consistent with the previous result for PS₂₀₀-*b*-PAA₄.²⁶ As the PS block length in copolymers increases, the diameters of copolymer micelles become larger. This can be ascribed to the higher degree of stretching of the core caused by the increased length of the insoluble block (PS) during micellization, which resulted in the increase in the size

of the formed micelles.³³ Encouraged by this result, we then explored the feasibility of synthesis of HMSNs using the spherical micelles of PS-*b*-PAA as core templates.

The SEM and TEM images of the synthesized HMSNs are shown in Fig. 3. The SEM images reveal that the obtained HMSNs are of spherical shape (Fig. 3a) and the crushed nanoparticles exhibit the hollow structure (Fig. 3b), while the TEM images in Fig. 3c–e also confirm the hollow structure of the resulting nanoparticles by respectively using different copolymers (PS₃₅-*b*-PAA₄, PS₅₈-*b*-PAA₄ and PS₁₁₃-*b*-PAA₄) and CTAB as co-templates. The magnified TEM image in Fig. 3f further reveals the worm-like mesoporous channels in the shell of the nanoparticles. These results demonstrated that the spherical micelles of amphiphilic block copolymers could be served as core-templates to synthesize the HMSNs. Based on the results described above, a possible formation mechanism of HMSNs templated by PS-*b*-PAA and CTAB was proposed (Fig. 4a). We speculate that PS-*b*-PAA was first to form spherical micelles with hydrophobic PS inside and hydrophilic PAA outside in the mixture solution of THF and H₂O. Then, in the presence of ammonia aqueous solution, the hydrophilic PAA blocks on the surface of spherical micelle aggregates could couple with CTAB *via* electrostatic interactions between PAA[−] and CTA⁺ to generate CTAB-coated PS-*b*-PAA aggregates, which is similar to the process proposed by Niu *et al.*³⁰ When TEOS molecules are added, they are consecutively hydrolyzed and assembled with CTAB by self-assembly, resulting in the silica growing on the surface of the micelles. After the removal of PS-*b*-PAA and CTAB by calcination, HMSNs were obtained.

Additionally, the size and morphology of the synthesized HMSNs can be influenced by the added amount of additives

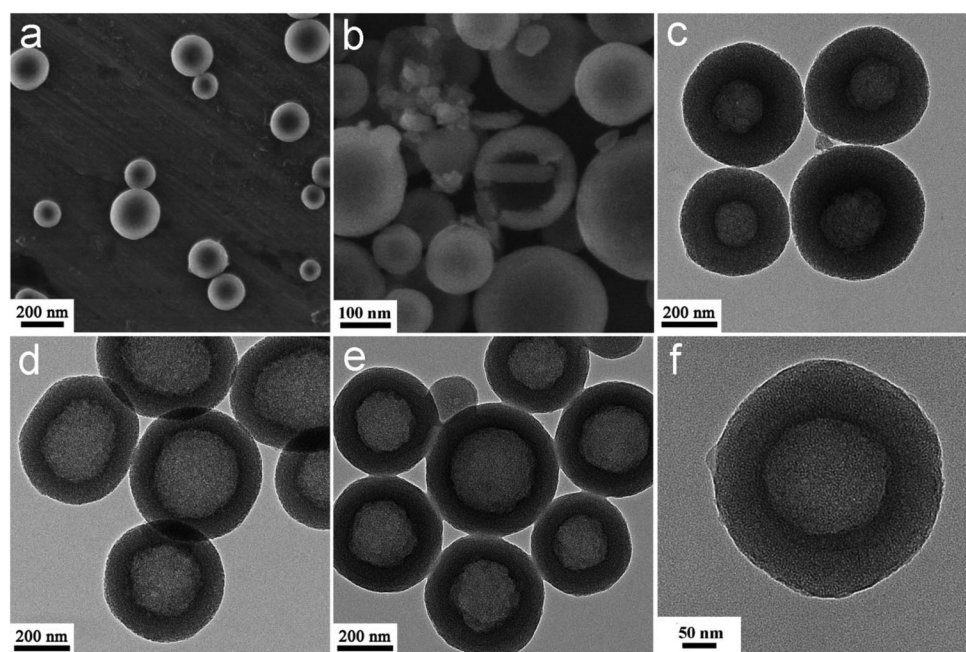


Fig. 3 (a) SEM image of as-prepared HMSNs. (b) SEM image of partially crushed HMSNs at high magnification. (c–e) TEM images of HMSNs prepared with PS₃₅-*b*-PAA₄, PS₅₈-*b*-PAA₄ and PS₁₁₃-*b*-PAA₄ respectively. (f) High-magnification TEM image of HMSNs.

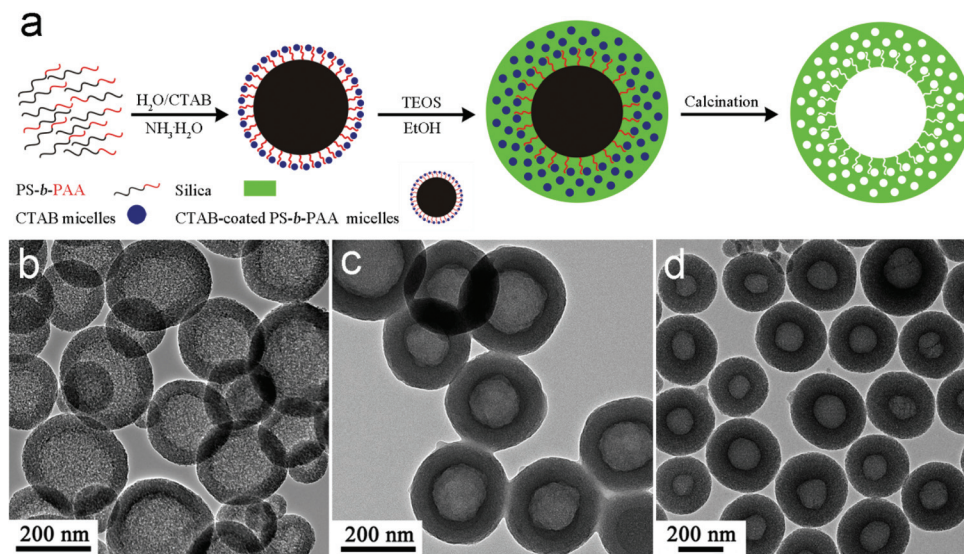


Fig. 4 (a) Schematic illustration of the formation of HMSNs. TEM images of HMSNs with different shell thicknesses prepared by adding different amounts of $PS_{35}\text{-}b\text{-}PAA_4$: (b) HMSN- $PS_{35}\text{-}a$, (c) HMSN- $PS_{35}\text{-}b$ and (d) HMSN- $PS_{35}\text{-}c$.

during the synthesis process. The previous studies have shown that the shell thickness of HMSNs can be easily controlled by changing the amount of TEOS.^{14,18,34} Therefore, we further investigate the effect of copolymer concentration on the size and morphology of HMSNs. Fig. 4b–d show the TEM images of HMSNs prepared with different amounts of $PS_{35}\text{-}b\text{-}PAA_4$. It can be seen that the synthesized HMSNs were uniform and spherical. Furthermore, an increase in the particle size of the HMSNs is observed when the amount of copolymer is decreased from 80 to 70 mg. The particle sizes of the HMSNs were measured by DLS (Fig. 5), which showed that the average diameter of all three samples was 231.6, 259.1 and 289.5 nm, respectively. Herein, they are denoted as HMSN- $PS_{35}\text{-}a$, HMSN- $PS_{35}\text{-}b$ and HMSN- $PS_{35}\text{-}c$, respectively. Concurrently, the shell thickness of HMSNs increased with the decrease in the

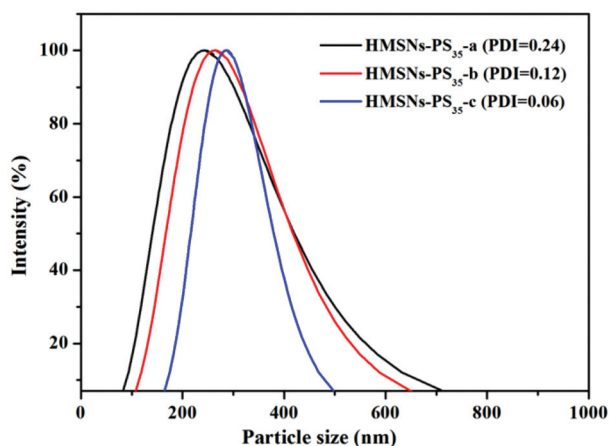


Fig. 5 Size distribution curves of HMSN- $PS_{35}\text{-}a$, HMSN- $PS_{35}\text{-}b$ and HMSN- $PS_{35}\text{-}c$.

added amount of $PS_{35}\text{-}b\text{-}PAA_4$, which was 46.0 ± 5.4 , 64.6 ± 4.7 and 82.2 ± 6.8 nm when the added amount of $PS_{35}\text{-}b\text{-}PAA_4$ was 80, 75 and 70 mg, respectively. The results may be due to the fact that the increased amount of copolymer results in the increase in the number of micelle aggregates, thereby causing a less silica condensation onto the surface of the each CTAB-coated $PS\text{-}b\text{-}PAA$ micelle. Fig. 6a shows the FT-IR spectrum of the calcined HMSNs (HMSN- $PS_{35}\text{-}c$). It gives a series of absorption bands, including 1090 and 803 cm^{-1} of Si–O–Si asymmetric stretching and symmetric stretching vibration, and 3405 and 965 cm^{-1} of hydroxyl groups and Si–O stretching vibration of Si–OH.^{13,35,36} In addition, Fig. 6b shows the small-angle XRD pattern of HMSN- $PS_{35}\text{-}c$. The XRD pattern indicates that the mesopores in the HMSNs are disordered, which is consistent with TEM observations.³⁷ The mesoporous structured shell of HMSNs was further characterized by nitrogen adsorption–desorption analysis. As shown in Fig. 7e, the nitrogen adsorption–desorption isotherms exhibit a typical type-IV curve, indicative of the mesoporous character of the HMSN samples.³⁸ The hysteresis loop in the range of $P/P_0 = 0.4\text{--}1.0$ reveals the hollow structure in the core of the HMSNs.¹² As shown in the inset in Fig. 7e, the mesoporous pore sizes of three samples are typically centered at about 4.0 nm, which are calculated by the BJH method. In addition, the particles with the larger particle size (HMSN- $PS_{35}\text{-}c$) exhibited a bimodal pore size distribution with additional micropores of a size less than 2 nm. The BET surface areas of HMSN- $PS_{35}\text{-}a$, HMSN- $PS_{35}\text{-}b$ and HMSN- $PS_{35}\text{-}c$ are calculated to be 985.6, 710.3 and 613.7 $\text{m}^2 \text{g}^{-1}$ respectively.

It is known that the surfactant (CTAB) is a critical additive in the formation of mesoporous silica materials. Without CTAB, $PS\text{-}b\text{-}PAA$ micelles and TEOS cannot self-assemble to form mesoporous silica materials.³⁰ Therefore, the effects of

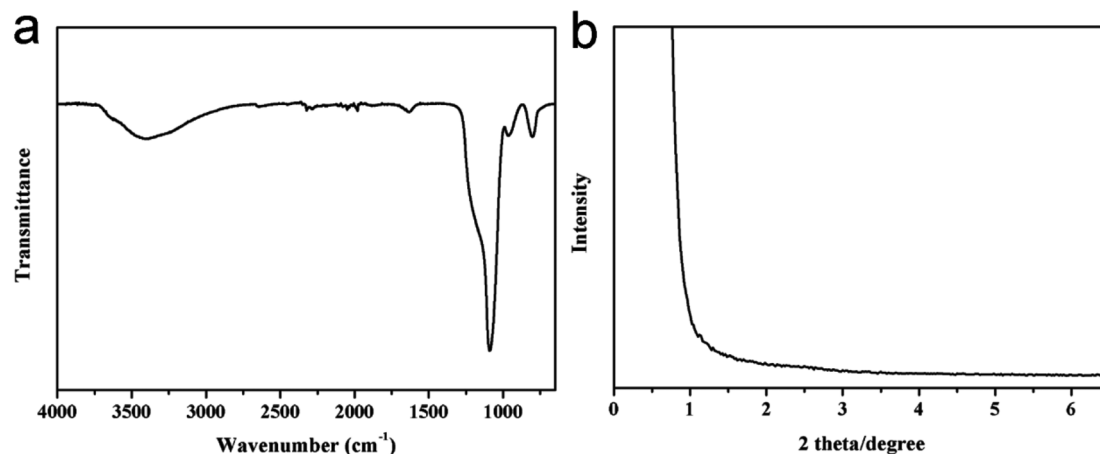


Fig. 6 (a) FT-IR spectrum of HMSN-PS₃₅-c. (b) Small-angle XRD pattern of HMSN-PS₃₅-c.

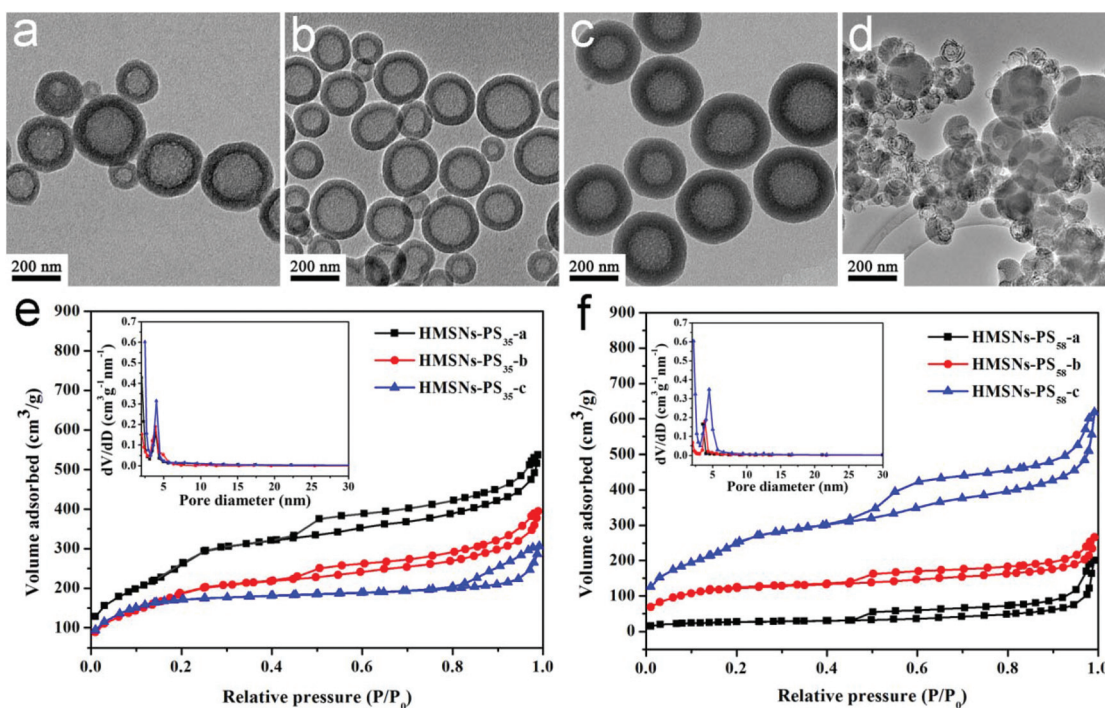


Fig. 7 TEM images of HMSNs with different pore sizes prepared by adding different amounts of CTAB: (a) HMSN-PS₅₈-a, (b) HMSN-PS₅₈-b (c) HMSN-PS₅₈-c and (d) HMSN-PS₅₈-d. Nitrogen adsorption-desorption isotherms and the inset pore size distribution curves of (e) different shell thicknesses of HMSNs and (f) different pore sizes of HMSNs.

CTAB on the structure and morphology of HMSNs were further investigated. Fig. 7a-c show the TEM images of HMSNs prepared using different amounts of CTAB, which indicated that the well-defined HMSNs can be synthesized as the amounts of CTAB increased from 160 to 200 mg. Herein, they are denoted as HMSN-PS₅₈-a, HMSN-PS₅₈-b and HMSN-PS₅₈-c, respectively. When the added amount of CTAB is 200 mg, uniform and well-dispersed nanoparticles were obtained (Fig. 7c). However, when the amount of CTAB reached 240 mg, the morphology of the resulting nanoparticles became disordered and poorly dis-

persed (Fig. 7d). The nitrogen adsorption-desorption isotherms of the obtained HMSNs (Fig. 7f) give the type-IV curves and H4-type hysteresis loops at a relative pressure (P/P_0) above 0.4, suggesting the presence of mesopores and a hollow cavity.^{10,12,13} As the added CTAB increased from 160 to 200 mg, the average mesoporous pore sizes calculated by the BJH method are 3.6, 3.9 and 4.5 nm, respectively (inset graph in Fig. 7f). These results indicate that the pore size of the resulting HMSNs can be tuned by changing the amount of CTAB.

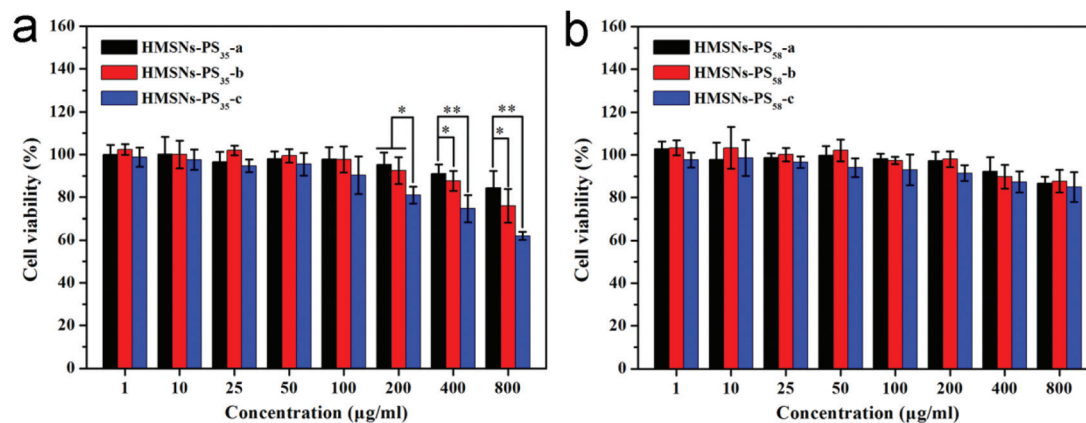


Fig. 8 Cell viability of HeLa cells after incubation with different concentrations of HMSNs for 24 h. (a) Different shell thicknesses of HMSNs and (b) different pore sizes of HMSNs.

In vitro cytotoxicity of HMSNs

To investigate the effects of the shell thickness and pore size of HMSNs on the cytotoxicity, cell viability against HeLa cells was examined by the CCK-8 assay. Fig. 8a shows the cell viability after incubating cells with three types of HMSNs (HMSN-PS₃₅-a, HMSN-PS₃₅-b and HMSN-PS₃₅-c) at different particle concentrations (1, 10, 25, 50, 100, 200, 400 and 800 $\mu\text{g ml}^{-1}$) for 24 h. As can be seen from Fig. 8a, all the nanoparticles showed a dose-dependent increase in their cytotoxicity despite different shell thicknesses. After incubating cells with HMSN-PS₃₅-a, the cell viability was still above 84% even at the highest nanoparticle concentration of 800 $\mu\text{g ml}^{-1}$, which indicated a low cytotoxicity. After incubating cells with HMSN-PS₃₅-b, cell viability was reduced from over 85% to 76% when the particle concentrations increased from 400 to 800 $\mu\text{g ml}^{-1}$. Furthermore, HMSN-PS₃₅-b shows statistically higher cytotoxicity ($P < 0.05$) than HMSN-PS₃₅-a at the particle concentration of 400 $\mu\text{g ml}^{-1}$. In contrast, HMSN-PS₃₅-c showed the highest cytotoxicity among the three types of nanoparticles when the particle concentration was above 400 $\mu\text{g ml}^{-1}$. As mentioned above, the shell thickness of three types of HMSNs is different. Therefore, the results suggested that an increase in the shell thickness of HMSNs resulted in an increased cytotoxicity, and the cytotoxicity of HMSNs was shell thickness- and dose-dependent. Considering that the synthesized HMSNs had the same size range of 230–290 nm, the effect of particle size on the cytotoxicity is very limited. Therefore, the difference in cytotoxic activity among various HMSNs can be explained by the fact that the nanoparticles with greater shell thickness probably contain more silanol groups than those with smaller shell thickness, thus inducing increased plasma membrane damage,³⁹ especially at high concentrations of nanoparticles. In contrast, the three kinds of HMSNs having different pore sizes (HMSN-PS₅₈-a, HMSN-PS₅₈-b and HMSN-PS₅₈-c) do not show apparent cytotoxicity within the measured concentrations (cell viability $\geq 85\%$), and there is no statistical difference among them (Fig. 8b), suggesting that the pore size of HMSNs has no direct effect on cytotoxicity.

Hemolysis assays of HMSNs

Hemolytic activity is one of the key indicators to evaluate the blood compatibility of blood-contacting materials such as particulate drug delivery systems. However, only a few work have so far been conducted to assess the hemolytic activity of HMSNs.^{20,40} To evaluate the cytotoxic effect of HMSNs with different shell thicknesses and pore sizes on human RBCs, the RBCs were exposed to each HMSN sample in the concentration range of 25 to 800 $\mu\text{g ml}^{-1}$ for 3 h. The hemolysis percentage of HMSN-treated RBCs was determined by measuring the absorbance of hemoglobin. As shown in Fig. 9a, the optical images present the direct observation of hemolysis at different concentrations of HMSNs. In Fig. 9c, it can be seen that almost no hemolysis of RBCs by HMSN-PS₃₅-a could be detected, only $4.8\% \pm 0.6$ of hemolysis percentage measured at the highest concentration of 800 $\mu\text{g ml}^{-1}$. But HMSN-PS₃₅-b and HMSN-PS₃₅-c exhibited a dose-dependent hemolytic activity which increased rapidly with the increase of particle concentration. Moreover, the hemolysis percentage of HMSN-PS₃₅-c reach $48.3 \pm 0.2\%$ at the concentration of 800 $\mu\text{g ml}^{-1}$, which is over 10-fold and 1.5-fold greater than that of HMSN-PS₃₅-a and HMSN-PS₃₅-b ($31.0 \pm 0.2\%$), respectively. The result demonstrated that the thicker shell resulted in higher hemolytic activity. Therefore, these results reveal a dose-dependent and shell thickness-dependent hemolytic activity of HMSNs with different shell thicknesses. The higher hemolytic activity of HMSNs with increased shell thickness may be due to their slightly larger particle size, which causes higher silanol density on the external surface of nanoparticles that was accessible to the RBCs, thus inducing increased damage to the RBC membrane.^{3,41} For three types of HMSNs with different pore sizes, no obvious hemolysis can be observed in the concentration range of 25–400 $\mu\text{g ml}^{-1}$ (Fig. 9b), while relatively low hemolysis percentages of $7.8 \pm 0.5\%$, $8.0 \pm 0.8\%$ and $8.7 \pm 1.0\%$ for HMSN-PS₅₈-a, HMSN-PS₅₈-b and HMSN-PS₅₈-c were measured when the particle concentration was 800 $\mu\text{g ml}^{-1}$ (Fig. 9d). These results demonstrated that the hemolysis by

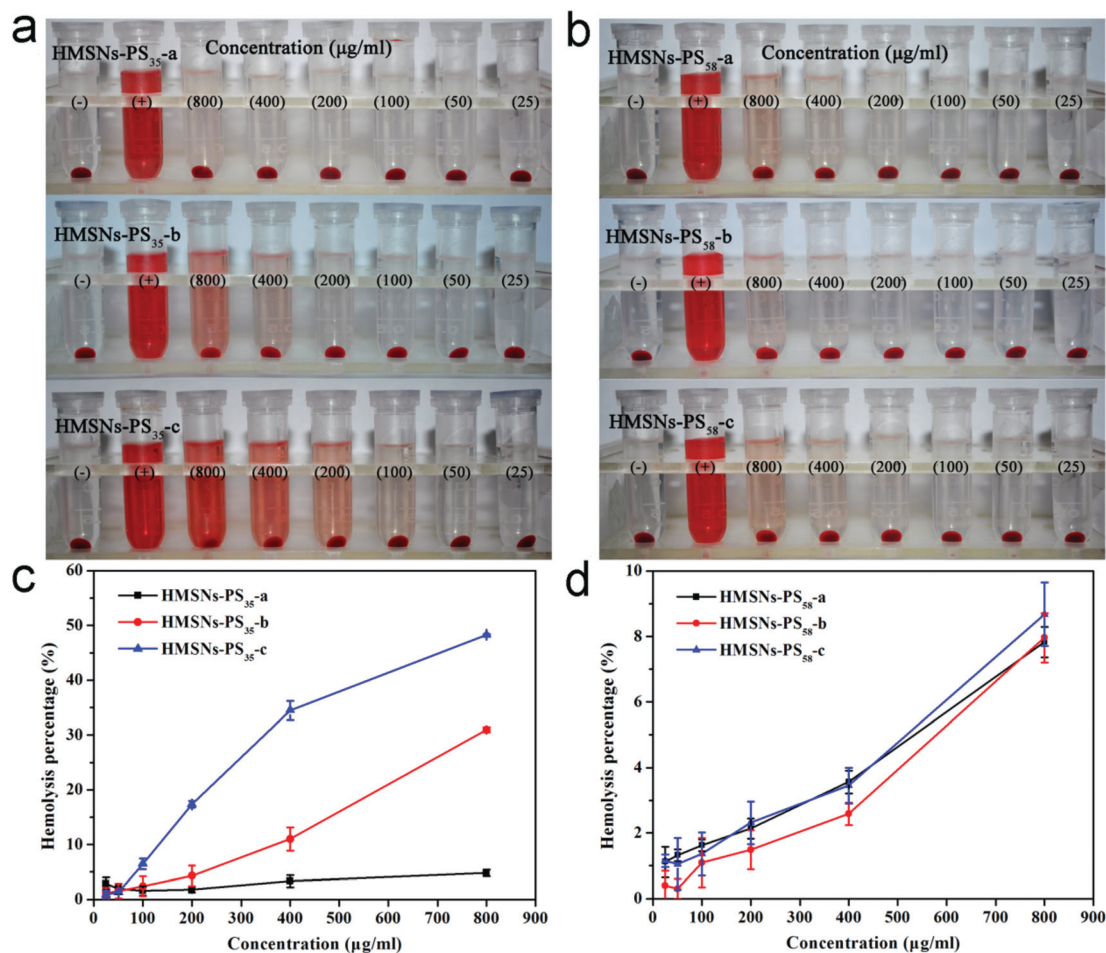


Fig. 9 Hemolysis assay of RBCs incubated with HMSNs of different shell thicknesses and pore sizes. (a, b) Photographic images and (c, d) hemolysis percentages of RBCs after HMSN sample exposure, using PBS as a negative control (-) and water as a positive control (+), the red blood cells are red due to the presence of hemoglobin.

HMSNs with different pore sizes is in a predominately dose-dependent manner.

Conclusions

In summary, we present a simple method to fabricate HMSNs with tunable shell thickness and pore size. Amphiphilic block copolymers of PS-*b*-PAA with different PS block lengths were synthesized *via* atom transfer radical polymerization; thus the prepared PS-*b*-PAA and CTAB were subsequently used as co-templates to synthesize HMSNs. The shell thickness and particle size of the resulting HMSNs can be tuned by changing the amount of PS-*b*-PAA and the amount of CTAB, respectively. The *in vitro* results indicated that the shell thickness of HMSNs had a significant effect on the cytotoxicity of HeLa cells, while the pore size had no obvious effect on the cytotoxicity. Hemolysis assays further revealed that HMSNs had a low hemolytic activity on RBCs. Therefore, the synthesized HMSNs hold considerable potential for future biomedical applications.

Acknowledgements

This work was financially supported by the National Natural Science Foundation of China (31271028), the Shanghai Nano Science Program (11nm0505500), the Innovation Program of Shanghai Municipal Education Commission (13ZZ051), the Chinese Universities Scientific Fund (CUSF-DH-D-2014019), and the Open Foundation of State Key Laboratory for Modification of Chemical Fibers and Polymer Materials (LK1202).

Notes and references

- 1 D. Zhao, *Science*, 1998, **279**, 548–552.
- 2 I. Slowing, J. Viveroescoto, C. Wu and V. Lin, *Adv. Drug Delivery Rev.*, 2008, **60**, 1278–1288.
- 3 W. Feng, X. Zhou, C. He, K. Qiu, W. Nie, L. Chen, H. Wang, X. Mo and Y. Zhang, *J. Mater. Chem. B*, 2013, **1**, 5886–5898.
- 4 C. Li, *Catal. Rev.*, 2004, **46**, 419–492.
- 5 X. Feng, *Science*, 1997, **276**, 923–926.

- 6 L. Zhang, C. Yu, W. Zhao, Z. Hua, H. Chen, L. Li and J. Shi, *J. Non-Cryst. Solids*, 2007, **353**, 4055–4061.
- 7 A. Popat, S. B. Hartono, F. Stahr, J. Liu, S. Z. Qiao and G. Qing Lu, *Nanoscale*, 2011, **3**, 2801–2818.
- 8 K. Qiu, C. He, W. Feng, W. Wang, X. Zhou, Z. Yin, L. Chen, H. Wang and X. Mo, *J. Mater. Chem. B*, 2013, **1**, 4601–4611.
- 9 J. Wang, Q. Xiao, H. Zhou, P. Sun, Z. Yuan, B. Li, D. Ding, A. C. Shi and T. Chen, *Adv. Mater.*, 2006, **18**, 3284–3288.
- 10 M. Li, C. Zhang, X.-L. Yang and H.-B. Xu, *RSC Adv.*, 2013, **3**, 16304–16307.
- 11 X. Du and J. He, *Nanoscale*, 2011, **3**, 3984–4002.
- 12 Y. Jiao, J. Guo, S. Shen, B. Chang, Y. Zhang, X. Jiang and W. Yang, *J. Mater. Chem.*, 2012, **22**, 17636–17643.
- 13 M. Sasidharan, H. Zenibana, M. Nandi, A. Bhaumik and K. Nakashima, *Dalton Trans.*, 2013, **42**, 13381–13389.
- 14 Z. Chen, D. Niu, Y. Li and J. Shi, *RSC Adv.*, 2013, **3**, 6767–6770.
- 15 Z. Feng, Y. Li, D. Niu, L. Li, W. Zhao, H. Chen, L. Li, J. Gao, M. Ruan and J. Shi, *Chem. Commun.*, 2008, **23**, 2629–2631.
- 16 Y. Zhao, L.-N. Lin, Y. Lu, S.-F. Chen, L. Dong and S.-H. Yu, *Adv. Mater.*, 2010, **22**, 5255–5259.
- 17 X. Mei, D. Chen, N. Li, Q. Xu, J. Ge, H. Li and J. Lu, *Microporous Mesoporous Mater.*, 2012, **152**, 16–24.
- 18 A. B. D. Nandiyanto, Y. Akane, T. Ogi and K. Okuyama, *Langmuir*, 2012, **28**, 8616–8624.
- 19 X. Guo, X. Liu, B. Xu and T. Dou, *Colloids Surf., A*, 2009, **345**, 141–146.
- 20 Y. Chen, H. Chen, L. Guo, Q. He, F. Chen, J. Zhou, J. Feng and J. Shi, *ACS Nano*, 2009, **4**, 529–539.
- 21 N. E. Botterhuis, Q. Sun, P. C. M. M. Magusin, R. A. van Santen and N. A. J. M. Sommerdijk, *Chem. – Eur. J.*, 2006, **12**, 1448–1456.
- 22 H. Djojoputro, X. Zhou, S. Qiao, L. Wang, C. Yu and G. Lu, *J. Am. Chem. Soc.*, 2006, **128**, 6320–6321.
- 23 X. F. Zhong, S. K. Varshney and A. Eisenberg, *Macromolecules*, 1992, **25**, 7160–7167.
- 24 Z. Lei and S. Bi, *J. Biotechnol.*, 2007, **128**, 112–119.
- 25 C. Wang, Y. Mao, D. Wang, Q. Qu, G. Yang and X. Hu, *J. Mater. Chem.*, 2008, **18**, 683–690.
- 26 L. Zhang and A. Eisenberg, *Science*, 1995, **268**, 1728–1731.
- 27 H. Shen and A. Eisenberg, *Macromolecules*, 2000, **33**, 2561–2572.
- 28 S. E. Burke and A. Eisenberg, *Langmuir*, 2001, **17**, 8341–8347.
- 29 L. Zhang and A. Eisenberg, *Polym. Adv. Technol.*, 1998, **9**, 677–699.
- 30 D. Niu, Z. Ma, Y. Li and J. Shi, *J. Am. Chem. Soc.*, 2010, **132**, 15144–15147.
- 31 Y. Kang and T. A. Taton, *Angew. Chem., Int. Ed.*, 2005, **44**, 409–412.
- 32 C. Allen, D. Maysinger and A. Eisenberg, *Colloids Surf., B*, 1999, **16**, 3–27.
- 33 L. Zhang and A. Eisenberg, *J. Am. Chem. Soc.*, 1996, **118**, 3168–3181.
- 34 Z. Ran, Y. Sun, B. Chang, Q. Ren and W. Yang, *J. Colloid Interface Sci.*, 2013, **410**, 94–101.
- 35 F. Chen and Y. Zhu, *Microporous Mesoporous Mater.*, 2012, **150**, 83–89.
- 36 S. K. Das, M. K. Bhunia, D. Chakraborty, A. R. Khudabukhsh and A. Bhaumik, *Chem. Commun.*, 2012, **48**, 2891–2893.
- 37 Y. Chen, H. Chen, D. Zeng, Y. Tian, F. Chen, J. Feng and J. Shi, *ACS Nano*, 2010, **4**, 6001–6013.
- 38 R. Pierotti and J. Rouquerol, *Pure Appl. Chem.*, 1985, **57**, 603–619.
- 39 T. Yu, A. Malugin and H. Ghandehari, *ACS Nano*, 2011, **5**, 5717–5728.
- 40 Y. Chen, P. Xu, H. Chen, Y. Li, W. Bu, Z. Shu, Y. Li, J. Zhang, L. Zhang, L. Pan, X. Cui, Z. Hua, J. Wang, L. Zhang and J. Shi, *Adv. Mater.*, 2013, **25**, 3100–3105.
- 41 Y.-S. Lin and C. L. Haynes, *J. Am. Chem. Soc.*, 2010, **132**, 4834–4842.